



This is a repository copy of *The 155-day X-ray cycle of the very massive Wolf-Rayet star Melnick 34 in the Large Magellanic Cloud.*

White Rose Research Online URL for this paper:
<http://eprints.whiterose.ac.uk/143768/>

Version: Published Version

Article:

Pollock, A.M.T., Crowther, P.A., Tehrani, K. et al. (2 more authors) (2018) The 155-day X-ray cycle of the very massive Wolf-Rayet star Melnick 34 in the Large Magellanic Cloud. *Monthly Notices of the Royal Astronomical Society*, 474 (3). pp. 3228-3236. ISSN 0035-8711

<https://doi.org/10.1093/mnras/stx2879>

This article has been accepted for publication in *Monthly Notices of the Royal Astronomical Society* ©: 2017 The Author(s). Published by Oxford University Press on behalf of the Royal Astronomical Society. All rights reserved.

Reuse

Items deposited in White Rose Research Online are protected by copyright, with all rights reserved unless indicated otherwise. They may be downloaded and/or printed for private study, or other acts as permitted by national copyright laws. The publisher or other rights holders may allow further reproduction and re-use of the full text version. This is indicated by the licence information on the White Rose Research Online record for the item.

Takedown

If you consider content in White Rose Research Online to be in breach of UK law, please notify us by emailing eprints@whiterose.ac.uk including the URL of the record and the reason for the withdrawal request.



eprints@whiterose.ac.uk
<https://eprints.whiterose.ac.uk/>

The 155-day X-ray cycle of the very massive Wolf–Rayet star Melnick 34 in the Large Magellanic Cloud

A. M. T. Pollock,¹* P. A. Crowther,¹ K. Tehrani,¹ Patrick S. Broos²
and Leisa K. Townsley²

¹Department of Physics and Astronomy, University of Sheffield, Hounsfield Road, Sheffield S3 7RH, UK

²Department of Astronomy & Astrophysics, 525 Davey Laboratory, Pennsylvania State University, University Park, PA 16802, USA

Accepted 2017 October 26. Received 2017 October 24; in original form 2017 August 24

ABSTRACT

The Wolf–Rayet star Mk 34 was observed more than 50 times as part of the deep T-ReX *Chandra* ACIS-I X-ray imaging survey of the Tarantula Nebula in the Large Magellanic Cloud conducted between 2014 May and 2016 January. Its brightness showed one bright maximum and repeated faint minima which help define an X-ray recurrence time of 155.1 ± 0.1 d that is probably the orbital period of an eccentric binary system. The maximum immediately precedes the minimum in the folded X-ray light curve as confirmed by new *Swift* XRT observations. Notwithstanding its extreme median luminosity of 1.2×10^{35} erg s⁻¹, which makes it over an order of magnitude brighter than comparable stars in the Milky Way, Mk 34 is almost certainly a colliding-wind binary system. Its spectrum shows phase-related changes of luminosity and absorption that are probably related to the orbital dynamics of two of the most massive stars known.

Key words: shock waves – binaries: eclipsing – stars: massive – stars: winds, outflows – stars: Wolf–Rayet – X-rays: stars.

1 INTRODUCTION

The Tarantula Nebula or 30 Doradus in the Large Magellanic Cloud is the most important star-forming complex in the Local Group. At its heart is R136, the stellar cluster that contains the most massive stars known (Crowther et al. 2010, 2016) which fall into the categories of O stars and more particularly hydrogen-rich Wolf–Rayet stars. Between 2014 and 2016, a high-spatial-resolution X-ray imaging survey known as T-ReX was undertaken with the *Chandra* Observatory to study both the stellar population itself and the thermal and dynamical effects wrought by stellar winds and supernova shocks on the surrounding interstellar medium.

The exposure time of 2 million seconds accumulated over nearly 21 months offers a far more intensive view of the stars in 30 Doradus than anything so far available for the Milky Way although there have been significant amounts of X-ray observing time on individual massive stars such as the nearby, single, early O-type supergiant ζ Puppis (e.g. Nazé, Flores & Rauw 2012), long used by *XMM–Newton* as a calibration source, and the more distant long-period binaries WR 140 (e.g. Pollock 2012) and η Carinae (e.g. Corcoran 2005). There is a clear physical distinction between the soft intrinsic X-ray emission produced in the winds of single stars, commonly attributed to many microscopic shocks supposed

by Feldmeier, Puls & Pauldrach (1997) and others to form as a consequence of instabilities in the wind-driving mechanism, and the harder, more luminous emission resulting from the macroscopic shock interaction between the counter flowing winds in a bound system of two or more massive stars (e.g. Stevens, Blondin & Pollock 1992; Rauw & Nazé 2016).

The variability properties of single and binary stars are also different. The *XMM–Newton* data of ζ Puppis collected intermittently over many years have shown stochastic variability of unknown origin of up to 10 per cent or so on time-scales of hours or days (Nazé, Oskinova & Gosset 2013) which appears typical of the intrinsic emission of single O stars in general. Among the binaries, on the other hand, the highly eccentric system WR 140, of 7.9-yr orbital period, shows changes in X-ray intensity many times higher determined mainly by the relative disposition of the two stars through orbital separation and stellar conjunction (e.g. Pollock 2012; Sugawara et al. 2015b). Closer binary systems with periods, P , of days rather than years, such as the Wolf–Rayet binary V444 Cygni (WN5o+O6III-V, $P = 4.2$ d), can show high-amplitude phase-repeatable X-ray variability, more complex than at longer wavelengths, where the hardness of the spectrum suggests colliding winds are involved (Lomax et al. 2015). On the other hand, X-ray emission from the prominent visual eclipsing O-star binary δ Orionis ($P = 5.7$ d) looked more like a single star in its behaviour during a simultaneous X-ray and optical campaign (Nichols et al. 2015) that covered most of an orbital cycle.

* E-mail: A.M.Pollock@sheffield.ac.uk

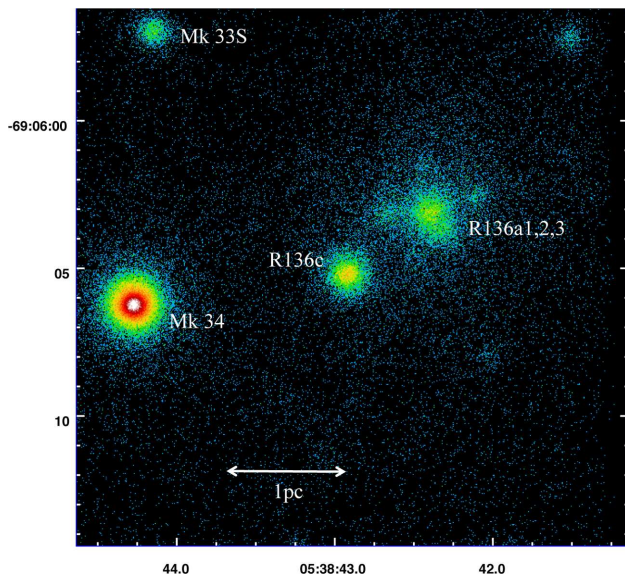


Figure 1. *Chandra* ACIS-I X-ray image on a logarithmic intensity scale of the core of 30 Doradus accumulated during the T-ReX campaign of an area of $19 \text{ arcsec} \times 19 \text{ arcsec}$ centred on R136c. North is up and east to the left. Also shown is the linear length-scale at the 50 kpc distance of the LMC.

For single and binary stars, variability in any part of the electromagnetic spectrum is an observational property of significance for determining the physical nature of a system. The T-ReX survey, which will be described in detail elsewhere, offers unprecedented opportunities of this type in the X-ray band. This paper concentrates on one particular star, Melnick 34 or BAT99 116, abbreviated Mk 34, near the centre of the broader survey. It lies 10 arcsec or 2.5 pc projected distance east of R136, the dense stellar core of 30 Doradus from which, as shown in Fig. 1, it is comfortably resolved by the *Chandra* telescope with the ACIS-I instrument which offers by far the best X-ray resolving power available now and in the foreseeable future.

Mk 34 is a hydrogen-rich Wolf–Rayet star, classified WN5ha by Crowther & Walborn (2011) or WN5h:a by Hainich et al. (2014), who assigned a high mass of $390 M_{\odot}$ through spectroscopic analysis. In the VLT-FLAMES census of the hot luminous stars in 30 Doradus (Doran et al. 2013), similar analysis suggested Mk 34 to be the second most luminous star behind R136a1 and to have the highest mass-loss rate of $6.3 \times 10^{-5} M_{\odot} \text{ yr}^{-1}$ among 500 confirmed hot stars, about 20 per cent higher than the estimate of Hainich et al. (2014). The colour index $B - V = 0.25$ shows that the star suffers significant extinction and X-ray absorption in the interstellar medium.

Through the discovery of dramatic optical radial-velocity variations that increased smoothly over 11 d only to have vanished a week later, Chené et al. (2011) established Mk 34, also designated P93_1134, to be a highly eccentric binary of two very massive stars. The data plotted in the middle panel of their fig. 1 suggest an orbital period greater than 50 d and a mass ratio of about 0.8.

Previous X-ray measurements showed it was the brightest stellar X-ray source in 30 Doradus, designated ACIS 132 of the 180 sources in the complete 1999 *Chandra* study of Townsley et al. (2006) and CX 5 of the 20 bright objects discussed by Portegies Zwart, Pooley & Lewin (2002). Before any published optical radial-velocity evidence, their common speculation was that Mk 34 is a binary with X-rays powered by colliding winds, this despite a luminosity about an order of magnitude higher than any comparable system in the

Milky Way and no evidence for variability, either in the *Chandra* data or in comparison with other measurements years earlier.

2 CHANDRA T-REX CAMPAIGN

The 51 observations of the *Chandra* Visionary Program (PI: Townsley) known as T-ReX, to signify the Tarantula – revealed by X-rays, were executed over 630 d between 2014 May 3 and 2016 January 22. They were all targeted at R136a1, the central star of the dense stellar core of 30 Doradus that lies 10 arcsec from Mk 34, and were executed at different spacecraft roll angles according to season. The ACIS-I field of view measures $16.9 \text{ arcmin} \times 16.9 \text{ arcmin}$ so that Mk 34 was always located in the central parts of the detector where the angular resolution is at its sharpest. The disposition of sources including Mk 34 with respect to detector edges or bad-surface geometry depends on the roll angle which thus partly determines detection sensitivity. Each observation was analysed with the ACIS EXTRACT package (Broos et al. 2010) used in previous work on stellar clusters, notably the *Chandra* Carina Complex Project (Broos et al. 2011; Townsley et al. 2011). For point sources such as Mk 34, the package delivers overall X-ray count rates and medium-resolution spectra with accompanying calibration material dependent on individual observing conditions to allow robust comparison of measurements taken at different times. For Mk 34 in this paper, the detected count rates were corrected according to the relative mean of the energy-dependent effective area tabulated for each observation in the ARF file, the so-called associated response function, which also encodes the instrumental geometry.

The observation log in Table 1 shows the sequence of sensitivity-corrected count rates for Mk 34 during the T-ReX campaign with three earlier archived observations from 2006 January bringing the total to 54.

As discussed by Broos et al. (2011) in their appendix A and Townsley et al. (2014), sources observed with the *Chandra* ACIS instrument are subject to pile-up in which two or more photons detected in identical or adjacent spatial and temporal readout elements are indistinguishable from single events with the energies combined. These are then either accepted or discarded according to a geometrical criterion known as grade selection. The outcome of these two effects is a reduction in the count rate that scales linearly with source brightness in Mk 34 and spurious hardening of the spectrum. For each X-ray source, the ACIS EXTRACT package provides simulated countermeasures in an overall count rate correction factor and a spectrum restored to remove pile-up distortion. Mk 34 has been bright enough during most of its *Chandra* observational history in Table 1 for pile-up to be significant: the count rate correction factor increases linearly with detected count rate to a maximum of 1.17 about a median of 1.08. While it is important to be aware of the extent of pile-up, the temporal analysis discussed below is most reliably done without pile-up corrections which have therefore not been applied to the count rates in Table 1. On the other hand, use of the reconstructed spectra is unavoidable for the X-ray spectroscopy considered below in Section 3.

2.1 *Chandra* X-ray photometry of Mk 34

The 54 observations of Mk 34 had exposure times between 9.8 and 93.7 ks about a median of 37.6 with count rates ranging between 2.2 and 76.2 counts per ks about a median of 35.8. The 51 count rates of Mk 34 during the 630-d T-ReX campaign itself are plotted in Fig. 2 and show obvious variability. This first became clear when two high measurements separated by 3 d in 2014 August at about twice the

Table 1. Log of *Chandra* observations in the T-ReX survey of 30 Doradus with observation ID and epoch; exposure time, T ; sensitivity factor relative to the ObsID 7263 maximum; sensitivity-corrected count rate per 1000 s of Mk 34; Kolmogorov–Smirnov variability test log-probability; and phase interval covered, ϕ , of the 155.1-d cycle centred on the X-ray maximum of 2014-08-22.

ObsID	Date	MJD	T (s)	Factor	Mk 34 (cts ks ⁻¹)	log P_{KS}	$\phi_{155.1}$ (d)
16192	2014-05-03T04:10:27	56780.174	93 761	0.95	35.9 ± 0.7	-0.152	+43.7 ⇔ +44.9
16193	2014-05-08T10:15:25	56785.427	75 994	0.95	35.6 ± 0.7	-0.003	+49.0 ⇔ +49.9
16612	2014-05-11T02:15:31	56788.094	22 672	0.96	35.4 ± 1.3	-0.430	+51.7 ⇔ +52.0
16194	2014-05-12T20:00:24	56789.834	31 333	0.93	38.9 ± 1.2	-0.732	+53.4 ⇔ +53.8
16615	2014-05-15T08:24:45	56792.351	45 170	0.96	35.4 ± 1.0	-0.068	+55.9 ⇔ +56.5
16195	2014-05-24T14:09:28	56801.590	44 405	0.93	33.7 ± 0.9	-0.040	+65.1 ⇔ +65.7
16196	2014-05-30T00:05:56	56807.004	67 109	0.96	35.8 ± 0.8	-0.296	+70.6 ⇔ +71.4
16617	2014-05-31T01:27:04	56808.060	58 860	0.93	33.5 ± 0.8	-0.255	+71.6 ⇔ +72.3
16616	2014-06-03T22:26:17	56811.935	34 530	0.93	35.9 ± 1.1	-0.205	+75.5 ⇔ +75.9
16197	2014-06-06T12:32:26	56814.523	67 790	0.95	34.8 ± 0.8	-0.292	-77.0 ⇔ -76.2
16198	2014-06-11T20:20:49	56819.848	39 465	0.93	31.1 ± 1.0	-0.393	-71.7 ⇔ -71.2
16621	2014-06-14T14:46:41	56822.616	44 400	0.93	34.7 ± 0.9	-0.203	-68.9 ⇔ -68.4
16200	2014-06-26T20:01:47	56834.835	27 361	0.94	36.5 ± 1.3	-0.078	-56.7 ⇔ -56.4
16201	2014-07-21T22:13:45	56859.926	58 390	0.93	42.0 ± 0.9	-0.171	-31.6 ⇔ -30.9
16640	2014-07-24T11:21:26	56862.473	61 679	0.93	44.1 ± 0.9	-0.018	-29.1 ⇔ -28.3
16202	2014-08-19T15:30:01	56888.646	65 128	0.93	70.7 ± 1.1	-0.313	-2.9 ⇔ -2.1
17312	2014-08-22T06:21:18	56891.265	44 895	0.93	76.2 ± 1.4	-0.346	-0.3 ⇔ +0.3
16203	2014-09-02T12:47:11	56902.533	41 423	0.94	2.4 ± 0.3	-0.014	+11.0 ⇔ +11.5
17413	2014-09-08T15:21:28	56908.640	24 650	0.94	21.6 ± 1.0	-0.151	+17.1 ⇔ +17.4
17414	2014-09-13T12:24:59	56913.517	17 317	0.94	35.2 ± 1.5	-0.078	+22.0 ⇔ +22.2
16442	2014-10-25T13:38:44	56955.569	48 350	0.93	34.9 ± 0.9	-1.161	+64.0 ⇔ +64.6
17545	2014-10-28T04:14:57	56958.177	34 530	0.93	32.7 ± 1.1	-0.086	+66.6 ⇔ +67.1
17544	2014-11-01T16:52:08	56962.703	25 642	0.93	35.9 ± 1.3	-0.326	+71.2 ⇔ +71.5
16443	2014-11-14T23:14:31	56975.968	34 530	0.93	33.6 ± 1.1	-0.322	-70.7 ⇔ -70.2
17486	2014-12-04T13:39:50	56995.569	33 541	0.92	36.7 ± 1.1	-0.353	-51.1 ⇔ -50.6
17555	2014-12-06T16:40:37	56997.695	55 247	0.90	35.8 ± 0.9	-0.017	-48.9 ⇔ -48.3
17561	2014-12-20T17:22:40	57011.724	54 567	0.93	38.6 ± 0.9	-0.154	-34.9 ⇔ -34.3
17562	2014-12-25T15:11:01	57016.633	42 031	0.92	43.5 ± 1.1	-0.293	-30.0 ⇔ -29.5
16444	2014-12-27T22:58:58	57018.958	41 440	0.88	42.9 ± 1.1	-1.282	-27.7 ⇔ -27.2
16448	2015-02-14T11:54:08	57067.496	34 599	0.95	34.4 ± 1.1	-1.223	+20.9 ⇔ +21.3
17602	2015-02-19T13:57:46	57072.582	51 705	0.95	37.0 ± 0.9	-0.130	+25.9 ⇔ +26.6
16447	2015-03-26T05:26:59	57107.227	26 868	0.94	34.2 ± 1.3	-1.138	+60.6 ⇔ +60.9
16199	2015-03-27T20:27:05	57108.852	39 461	0.94	35.3 ± 1.0	-0.853	+62.2 ⇔ +62.7
17640	2015-03-31T13:14:43	57112.552	26 318	0.92	37.3 ± 1.3	-0.807	+65.9 ⇔ +66.2
17641	2015-04-04T19:45:40	57116.823	24 638	0.95	32.3 ± 1.2	-0.456	+70.2 ⇔ +70.5
16445	2015-05-27T00:18:12	57169.013	49 310	0.95	39.0 ± 0.9	-0.412	-32.7 ⇔ -32.1
17660	2015-05-29T14:55:28	57171.622	38 956	0.95	42.0 ± 1.1	-0.202	-30.1 ⇔ -29.6
16446	2015-06-02T11:50:14	57175.493	47 547	0.95	42.6 ± 1.0	-0.316	-26.2 ⇔ -25.7
17642	2015-06-08T05:11:14	57181.216	34 438	0.92	49.3 ± 1.3	-0.584	-20.5 ⇔ -20.1
16449	2015-09-28T05:35:14	57293.233	24 628	0.92	34.3 ± 1.3	-0.127	-63.6 ⇔ -63.3
18672	2015-11-08T01:04:22	57334.045	30 574	0.92	46.4 ± 1.3	-0.291	-22.8 ⇔ -22.4
18706	2015-11-10T17:09:59	57336.715	14 776	0.92	44.9 ± 1.9	-0.068	-20.1 ⇔ -19.9
18720	2015-12-02T10:49:02	57358.451	9832	0.51	57.8 ± 3.8	-0.922	+1.6 ⇔ +1.7
18721	2015-12-08T17:13:14	57364.718	25 598	0.74	2.2 ± 0.4	-0.067	+7.9 ⇔ +8.2
17603	2015-12-09T15:27:36	57365.644	13 778	0.71	2.2 ± 0.6	-0.332	+8.8 ⇔ +9.0
18722	2015-12-11T09:09:39	57367.382	9826	0.62	4.6 ± 1.1	-0.739	+10.5 ⇔ +10.7
18671	2015-12-13T23:41:12	57369.987	25 617	0.55	12.2 ± 1.0	-0.234	+13.1 ⇔ +13.5
18729	2015-12-21T22:10:30	57377.924	16 742	0.74	33.6 ± 1.7	-2.099	+21.1 ⇔ +21.3
18750	2016-01-20T00:41:30	57407.029	48 318	0.85	34.8 ± 0.9	-5.557	+50.2 ⇔ +50.8
18670	2016-01-21T20:59:37	57408.875	14 565	0.63	35.7 ± 2.1	-0.758	+52.0 ⇔ +52.2
18749	2016-01-22T16:14:19	57409.677	22 153	0.56	32.1 ± 1.7	-0.423	+52.8 ⇔ +53.1
5906	2006-01-21T19:04:02	53756.794	12 317	1.00	39.2 ± 1.9	-0.992	-32.7 ⇔ -32.6
7263	2006-01-22T16:51:51	53757.703	42 528	1.00	41.6 ± 1.0	-0.169	-31.8 ⇔ -31.3
7264	2006-01-30T15:06:27	53765.629	37 593	0.98	41.5 ± 1.1	-0.885	-23.9 ⇔ -23.5

median were followed 11 d later by a measurement close to zero and further 6 d later at about half the median. A second minimum stretching over about a week in 2015 December and other brighter measurements in Fig. 2 strongly suggest four cycles of repeatable structure in the course of the 630-d T-ReX campaign.

Given the irregular sampling of the light curve, a more precise value was explored through minimum string-length analysis of the quantities

$$\{x_i, y_i\} = \{r_i \cos \phi_i, r_i \sin \phi_i\},$$

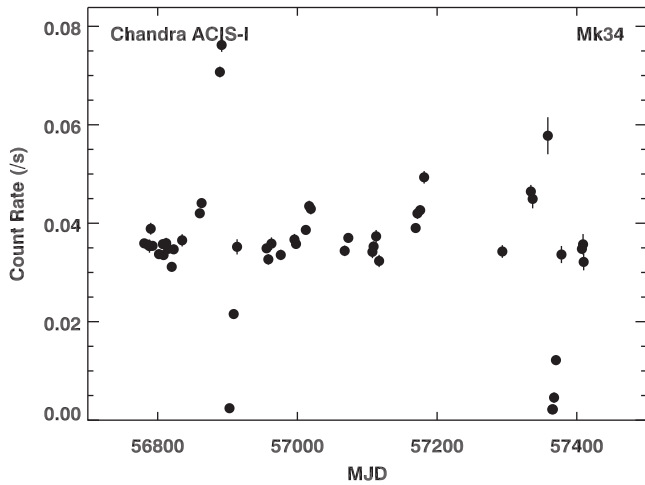


Figure 2. *Chandra* ACIS-I X-ray count rates of Mk 34 during the T-ReX campaign. Many of the error bars are smaller than the plot symbol.

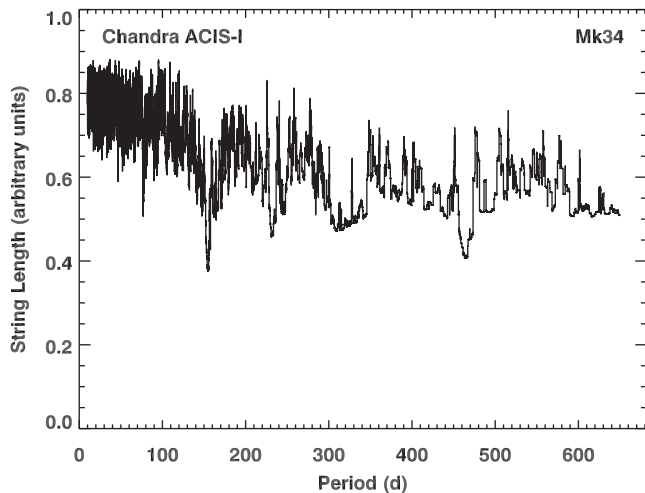


Figure 3. String length against trial period for the 54 *Chandra* ACIS-I X-ray count rate measurements of Mk 34 in Table 1.

where r_i is the count rate of the i th measurement ordered in folded phase of a trial period. The results are plotted in Fig. 3. The minimum value of the string-length curve infers a best-value period of 155.1 d with an uncertainty of 1 or 2 d. We also considered the Plavchan algorithm (Plavchan et al. 2008) implemented by the NASA Exoplanet Archive.¹ Although this method is considered by its authors better suited to the detection of small-amplitude variations among much more numerous data than available for Mk 34, it gave similar results.

The folded light curve with $P = 155.1$ d is shown in Fig. 4, where the maximum count rate was taken to define zero phase. The folded light curve shows accurate repeatability: despite some missing coverage, the light curve clearly shows an accelerating 30- or 40-d rise to maximum, followed by a sharp decrease in a few days to a minimum that lasts a few days, before a steady 10-d recovery to a relatively stable state of probably more than 100 d in length. Count rates plotted in grey from the archived observations over 10 d in late 2006 January agree within small errors with those close in phase taken 8–10 yr later as the rise began to accelerate. The decrease

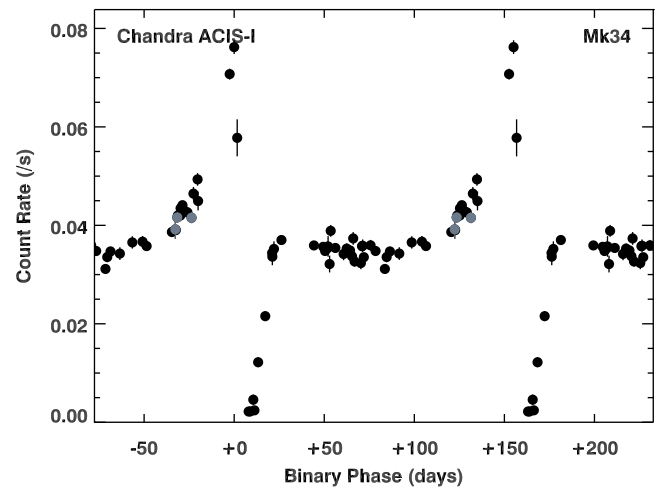


Figure 4. Repeated cycles of *Chandra* ACIS-I X-ray count rates of Mk 34 folded at the period of 155.1 d derived from string-length analysis centred on X-ray maximum. The points plotted in grey are those from the three archived observations in 2006 January, 8 or more years before the other data.

after maximum appears very steep: in the folded light curve, the closest measurements were 1.6 and 7.9 d later when the count rate had fallen by factors of 1.3 and more than 30, respectively.

There is little evidence for rapid variability within individual observations as shown by the modest values of $\log P_{KS}$ reported in Table 1, where P_{KS} is the P -value for the one-sample Kolmogorov–Smirnov statistic under the hypothesis of constant source flux.

2.2 X-ray historical record

The *XMM-Newton* science archive² shows that Mk 34 has been detected three times by the EPIC imaging spectrometers with the count rates reported in Table 2 during observations of PSR J0537-6909 in 2001 November, IGR J05414-6858 in 2011 October and in one exposure in 2012 October of the 48 forming a wide-area survey of the LMC. The three EPIC instruments, pn, MOS1 and MO2, observe simultaneously and cover nearly identical fields of view although Mk 34 was not observed by the pn instrument in 2001 November because of the timing mode chosen for the pulsar or by the MOS instruments in 2011 October because the star fell very close to the edge of the pn field of view where MOS coverage does not reach. Despite these complications, the *XMM* measurements of Mk 34, whose identification is confused as 3XMM J053843.[79]-690605 in the 3XMM-DR6 catalogue, showed clear variability by about a factor of 2 very well correlated with the *Chandra* folded light curve as shown by comparison with the ACIS-I count rates closest in phase also reported in Table 2. The three observations all took place in the rising part of the X-ray light curve with the 2001 measurement, the brightest of the three, a few days before maximum light 30 cycles earlier than the T-ReX maximum suggesting an uncertainty in the period of the order of 0.1 d.

2.3 New *Swift* X-ray photometry

Once the T-ReX campaign had finished, Mk 34’s putative period of 155.1 d was used to predict the timing of the next maximum in early

¹ <http://exoplanetarchive.ipac.caltech.edu>

² <http://nxsa.esac.esa.int/nxsa-web/#search>

Table 2. Log of *XMM-Newton* observations of Mk 34 with observation ID and epoch; exposure time, T ; detected XSA PPS count rate per 1000 s; phase interval covered, ϕ , of the 155.1-d cycle; and ACIS-I count rate from the nearest *Chandra* observation in phase.

Rev	ObsID	Date	MJD	T (s)	EPIC-pn (cts ks ⁻¹)	EPIC-MOS1 (cts ks ⁻¹)	EPIC-MOS2 (cts ks ⁻¹)	$\phi_{155.1}$ (d)	ACIS-I (cts ks ⁻¹)
0357	0113020201	2001-11-19	52232.9	38 159	...	124.4 ± 2.5	125.0 ± 2.5	−5.6 ⇔ −5.2	70.7 ± 1.1
2138	0679380101	2011-08-13	55786.3	24 268	275.5 ± 18.5	−19.5 ⇔ −19.3	44.9 ± 1.9
2358	0690744401	2012-10-23	56223.8	38 159	192.2 ± 4.7	64.8 ± 2.7	66.4 ± 2.7	−47.4 ⇔ −46.9	35.8 ± 0.9

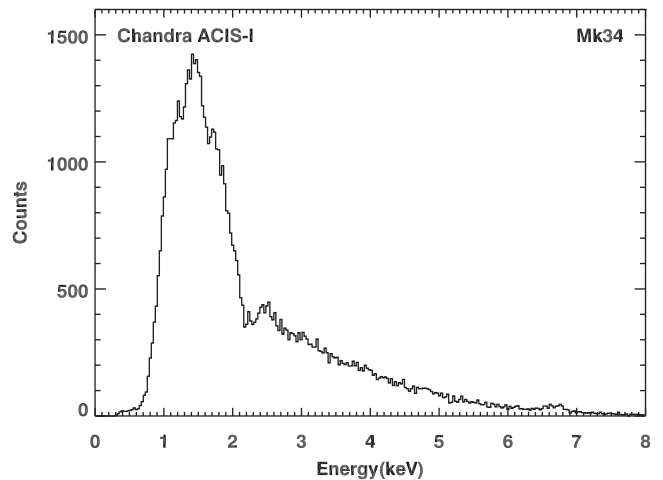
Table 3. Log of *Swift* ToO XRT observations of Mk 34 near the predicted maximum in 2016 May with observation ID and epoch; exposure time, T ; detected XRT count rate per 1000 s; and phase interval covered, ϕ , of the 155.1-d cycle.

Target	ObsID	Date	MJD	T (s)	XRT (cts ks ⁻¹)	$\phi_{155.1}$ (d)
Mk 34	00034533002	2016-05-03	57511.3	7085	38.8 ± 2.9	−0.63 ⇔ +0.06
Mk 34	00034533003	2016-05-10	57518.1	2566	6.0 ± 2.4	+6.15 ⇔ +6.95
SNR N157B	00081912001	2016-05-10	57518.2	955	10.3 ± 4.0	+6.28 ⇔ +6.36
Mk 34	00034533004	2016-05-11	57519.2	3481	8.2 ± 2.3	+7.28 ⇔ +8.02
Mk 34	00034533005	2016-05-15	57523.1	2469	7.4 ± 2.6	+11.13 ⇔ +12.13
Mk 34	00034533006	2016-05-31	52232.9	787	9.0 ± 5.0	+27.71 ⇔ +27.90
Mk 34	00034533007	2016-06-05	52232.9	6834	19.9 ± 2.1	+32.98 ⇔ +34.01

2016 May. With the recognition that the source is strong enough for sufficiently accurate measurements in reasonable exposures with the *Swift* XRT instrument in imaging PC mode, an application for *Swift* ToO observations was submitted and approved to cover the anticipated maximum and subsequent minimum at intervals of about 7 d. The results are shown in Table 3 where the sequence of detected count rates confirms the expectations based on the *Chandra* folded light curve in Fig. 4: the highest count rate detected on 2016 May 3 within hours of the predicted maximum was about twice as bright as the measurement about a month later. The much lower intervening count rates did not match the reductions of factors of 30 or so observed with *Chandra*, probably because of source confusion within the more modest angular resolution of the XRT which, in common with any other current X-ray instrument, does not match that of ACIS images. The *Swift* XRT images show two clearly resolved sources coincident with Mk 34 and R140a that are separated by 54 arcsec but cannot distinguish between Mk 34 and R136c only 7 arcsec away but a median factor of 8.6 fainter in resolved *Chandra* images.

3 CHANDRA X-RAY SPECTROSCOPY OF MK 34

The accumulated moderate resolution ACIS-I X-ray spectrum of Mk 34 shown in Fig. 5 gives a clear qualitative picture of its general spectral properties. The spectrum is hard, stretching beyond the clear detection of Fe_{XXV} at 6.7 keV with the presence of a strong continuum in addition to emission lines at all energies. This type of spectrum is characteristic of well-established colliding-wind binaries such as WR 140 (e.g. Pollock et al. 2005), WR 25 (e.g. Pollock & Corcoran 2006) and η Carinae although, given the 50 kpc distance of the LMC, Mk 34 is more luminous. In comparison with WR 25 at about 2.3 kpc in Carina, for example, Mk 34 is more than 20 times farther away and normally only 10 times fainter, suggesting a luminosity greater by roughly an order of magnitude. The much weaker intrinsic emission of some single Wolf–Rayet stars such as WR 78 (Skinner et al. 2010) and WR 134 (Skinner et al. 2012) also shows He-like line emission of Fe_{XXV} from very hot plasma but with no obvious continuum which therefore appears to be an important defining property of colliding winds. At low energies, the

**Figure 5.** *Chandra* ACIS-I X-ray spectrum of Mk 34 accumulated from all the available data.

spectrum of Mk 34 is marked by a steep cut-off below about 1 keV, likely due to a combination of circumstellar and interstellar photoelectric absorption, leaving little flux at the energies most affected by the instrumental contamination discussed below.

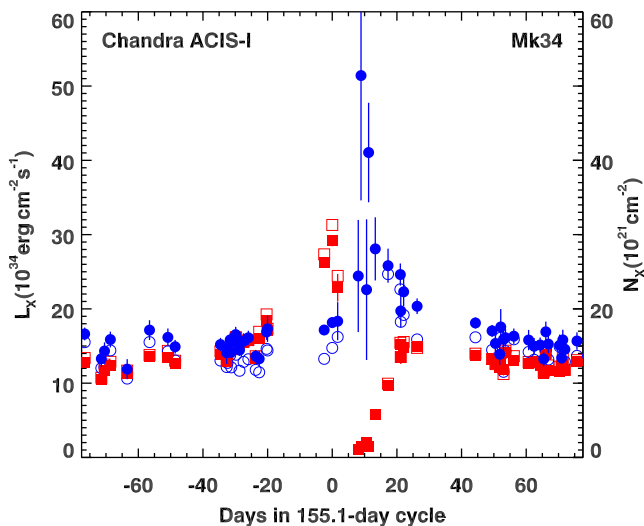
Each of the 54 individual spectra that contribute to Fig. 5 is accompanied by customized response files that reflect the contemporary calibration of the ACIS instrument and enable detailed models of the observed spectra to be constructed. Of particular relevance is knowledge of the instrumental contamination³ that affects most the sensitivity at low energies and has been building up in the ACIS optical path since launch in 2000 and has been developing more quickly since late 2009. These considerations are less important in Mk 34 than in objects with softer spectra.

Independent of count rate or phase, the shapes of all 54 spectra were very similar in shape. For each 0.5–8 keV spectrum, ACIS EXTRACT calculates the mean observed energy, $\langle E \rangle$, of its constituent events. The set of these values has a narrow distribution

³ <http://cxc.harvard.edu/ciao/why/acisqcontam.html>

Table 4. Best-fitting XSPEC reference plasma emission model of Mk 34.

$A_1 \text{vapec}(kT_1) + A_2 \text{vapec}(kT_2)$	
kT_1	1.198 ± 0.040 keV
A_1	$2.251 \pm 0.314 \times 10^{-4}$ cm $^{-5}$
kT_2	4.460 ± 0.209 keV
A_2	$4.675 \pm 0.219 \times 10^{-4}$ cm $^{-5}$
Ne	$0. \pm 0.072$
Mg	0.552 ± 0.125
Al	$0. \pm 0.330$
Si	0.756 ± 0.094
S	0.742 ± 0.100
Ar	0.727 ± 0.305
Ca	0.109 ± 0.402
Fe	0.336 ± 0.029

**Figure 6.** Phase-dependent *Chandra* ACIS-I estimates of the X-ray luminosity, L_X , in red squares and absorption, N_X , in blue circles of Mk 34 in units characteristic of colliding-wind systems in the Milky Way. The filled symbols with error bars show estimates ignoring pile-up; the open symbols without error bars were derived from spectra reconstructed to remove the effects of pile-up.

characterized by a mean absolute deviation of 0.042 keV about a median of 2.238 keV. The brightest and second brightest observations had $\langle E \rangle = 2.284$ keV and $\langle E \rangle = 2.305$ keV, respectively, comfortably within the overall distribution. Only the faintest spectra immediately after maximum were significantly harder probably due to increased photoelectric absorption, as discussed below.

Spectral models were fitted with XSPEC v12.6.0v simultaneously to all 54 spectra consisting of a constant empirical emission spectrum modified by 54 time-dependent values of luminosity, L_X , and absorbing column density, N_X , of LMC abundances. The emission was modelled with a two-temperature thermal plasma of variable abundances with the best-fitting parameters shown in Table 4. The purpose of the model is not to imply the simultaneous presence of two equilibrium plasmas of distinct temperature or to study the abundances but instead accurately to reproduce on a phenomenological basis the shape of the underlying spectrum in order to assess the evolution of luminosity and absorption.

The 54 values of L_X and N_X are plotted in Fig. 6 in units characteristic of familiar colliding-wind binary systems in the Galaxy of 10^{34} erg s $^{-1}$ and 10^{21} cm $^{-2}$ for luminosity and column density, re-

spectively. In Mk 34, both show coherent repeatable behaviour as a function of phase. Fig. 6 also suggests how pile-up has distorted the observed spectra by plotting with open symbols the values of L_X and N_X derived instead from analysis of the set of pile-up restored spectra supplied by ACIS EXTRACT. Recalling that pile-up affects typically 8 per cent and up to 17 per cent of counts by discarding or moving them to higher energies, apparent hardening of the spectrum of Mk 34 at its brightest which might have been thought due to increasing absorption was more likely caused by pile-up.

Mk 34 is an order of magnitude more luminous than any similar Galactic system. After apastron, its luminosity increases slowly at first before accelerating to reach a maximum brighter by a factor of about 3 that immediately precedes an event that looks like an eclipse. Within the limits of the data available, the steady recovery is reproducible between cycles and shows a sharp transition at +20 d after periastron to the gentle decrease that leads again to apastron.

The lack of colour variations throughout most of the orbit suggests that a constant interstellar component might account for most of the absorption observed in most of the spectra with a value of about 15×10^{21} cm $^{-2}$ according to Fig. 6. This is indeed consistent with expectations from Mk34's optical and IR photometry which shows some of the highest reddening among the hot stars in 30 Doradus. For the narrow-band colour excess $E(B - V)$, Doran et al. (2013) reported a value of 0.47 compared to 0.75 from the models of Hainich et al. (2014). For the elevated gas-to-dust ratio in R136 cited by Doran et al. (2013) and the low metallicity of the LMC, $Z = 0.5$, also used in the X-ray absorption model, this would imply an interstellar hydrogen column density of 11 or 17×10^{21} cm $^{-2}$ for the competing values of $E(B - V)$, bracketing the X-ray value.

Although through most of the orbit there is little evidence of X-ray colour changes, absorption does reach a maximum of about double the interstellar value for 2 or 3 weeks centred about 10 d after X-ray maximum during the single X-ray eclipse revealed by the light curve when one of the stars is probably passing across the line of sight. Here, low count rates make some estimates uncertain although there are some more precise measurements after eclipse egress. Another task of future observations with more complete phase coverage will be to try to identify a second eclipse.

4 FORM OF THE X-RAY LIGHT CURVE

The distinctive shape of the folded X-ray light curve of Mk 34 is very similar in phased form to that seen recently in the Galactic very massive Wolf–Rayet colliding-wind binary system WR 21a (Sugawara et al. 2015a; Gosset & Nazé 2016) with a combination of 100 ks of *XMM-Newton* data at four phases and 306 ks of a *Swift* ToO XRT campaign of 330 snapshots spread evenly over the entire 31.672-d period of its optical radial velocity orbit (Niemela et al. 2008; Tramper et al. 2016). A comparison of the two stars is shown in Fig. 7 where Mk 34's zero phase was shifted forward 10 d from its observed maximum count rate and the *Swift* XRT count rate was halved. Despite the differences in period of a factor of 5 and luminosity of more than an order of magnitude, the similarities are striking in the gradual rise to maximum followed by the subsequent deep minimum and asymmetric recovery. The well-established spectral types of WR 21a, O3/WN6ha+O3Vz((f*)), and its Keplerian orbital elements (Tramper et al. 2016) allow an assessment of the relationship between X-ray orbital light-curve morphology and stellar and orbital geometry as discussed in part by Gosset & Nazé (2016). Its minimum is probably caused, qualitatively at least, by some combination of three mechanisms: absorption by the extended wind of the Wolf–Rayet star, eclipse by its stellar

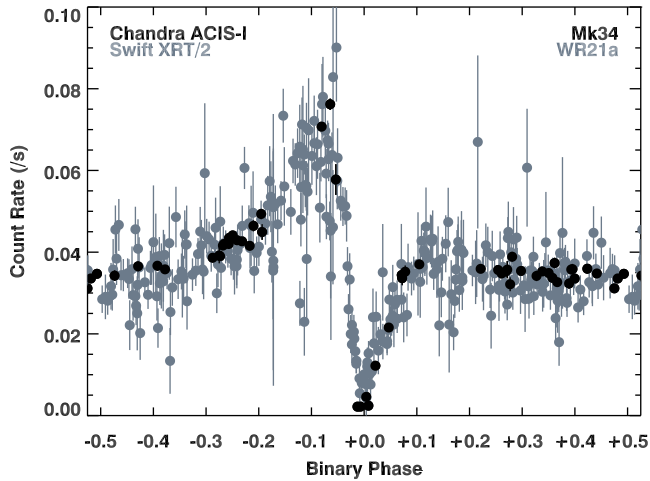


Figure 7. Phase-dependent *Chandra* ACIS-I X-ray count rate of Mk 34 in comparison with the *Swift* XRT light curve of the Galactic Wolf-Rayet eccentric binary system WR 21a after setting zero phase of Mk 34 10 d after its X-ray maximum.

core and reduced upstream shock velocities. The potential utility of X-ray measurements is emphasized by the lack of eclipses at longer wavelengths although quantitative models remain to be devised.

Once Mk 34's orbit is known in the near future, such quantitative models would seem to be required as simple arguments, although hard to fault, appear to fail: if the similarity of their X-ray light curves were to suggest similar orbital eccentricities for Mk 34 and WR 21a, then, as demanded by Kepler's laws, scaling the sum of WR 21a's minimum masses of $102 \pm 6 M_{\odot}$ (Tramper et al. 2016) by the period ratio and the cube of the relative velocity amplitudes according to Chené et al. (2011) would suggest unfeasibly high combined minimum masses of over $1000 M_{\odot}$ for Mk 34.

Mk 34 and WR 21a are not the only binary systems with very massive Wolf-Rayet primary stars that show high-amplitude orbital phase-related X-ray variability of apparently similar type. Of Crowther & Walborn's (2011) very massive stars, WR 25 in Carina and WR 43c in NGC 3603 are two other clear but more complex examples. The binary properties of the four systems, with periods ranging from about 10 to 200 d, are shown in Table 5 which also includes rough estimates of the X-ray luminosities at apastron, when the stars are farthest apart; at X-ray maximum, often close to periastron; and at eclipse minimum. Phased X-ray light curves are plotted in Fig. 8 scaled by distance to show their relative luminosities. *Swift* XRT data of WR 21a and WR 25 were scaled by a factor of 4 calculated from comparison of the ACIS-I count rate during

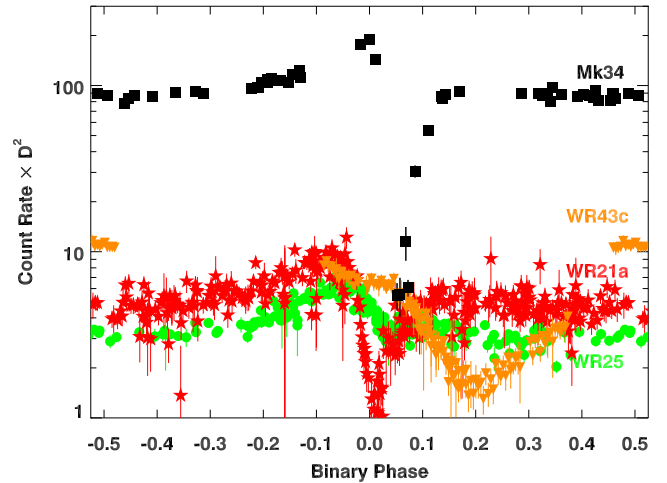


Figure 8. Phase-dependent ACIS-I X-ray count rate multiplied by the square of the distance in kpc of Mk 34 in comparison with three other X-ray bright binary systems in the Galaxy with very massive Wolf-Rayet primary stars.

the observation of WR 21a with ObsID 9113 with similar phases of the XRT light curve.

Mk 34 is the most luminous by about an order of magnitude, probably signalling the presence of two extreme stars in close proximity with high mass-loss rates and high-velocity winds. Repeatable events with all the appearance of eclipses occur in all four systems. For the well-established orbits of WR 21a and WR 25, these occur very close to inferior conjunction when the primary Wolf-Rayet star is passing in front of its binary companion and presumably also, therefore, in front of the X-ray source between the two stars. Like Mk 34, both these stars also show increased X-ray absorption in narrow intervals around these phases. These do not apply to the system of shortest period, WR 43c (Schnurr et al. 2008), one of the central stars in the cluster NGC 3603, where the smoother minimum rather occurs near a quadrature. As argued above, once orbital geometry has been defined by Kepler's laws, X-ray eclipses by star and wind promise direct estimates of fundamental parameters such as orbital inclination, stellar radius and mass-loss rate such as attempted, for example, by Pollock (2012) for WR 25. The data shown here for WR 25 and WR 43c will be discussed in detail elsewhere.

Luminous colliding-wind X-ray sources of high-amplitude orbital-driven variability are by no means ubiquitous among very massive Wolf-Rayet binary systems. The close binary WR 43a (WN6ha+WN6ha, $P = 3.7724$ d) in NGC3603 (Schnurr et al. 2008) is normally less luminous in X-rays than its neighbour WR 43c. Also

Table 5. Properties of Mk 34 and other colliding-wind systems.

System	Spectral type	Cluster	Distance (kpc)	Period (d)	e	L_X (10^{34} ergs $^{-1}$)		
						\Rightarrow	\uparrow	\downarrow
Mk 34	WN5ha + WN5ha	30 Doradus	50.	155.1	–	12.	32.	1.
WR 43c	O3If*/WN6 + ?	NGC 3603	7.6	8.89	0.30	0.9	–	0.1
WR 21a	O2.5If*/WN6ha + OVz((f*))	(Westerlund 2)	4.16	31.672	0.6949	0.6	1.2	0.1
WR 25	O2.5If*/WN6 + ?	Trumpler 16	2.3	207.808	0.4458	0.4	0.9	0.4
η Carinae	LBV + (WR)	Trumpler 16	2.3	2202.7	0.9	3.8	26.	0.2
WR 48a	WC8 + (O)	G305	4.0	12000.	–	1.9	–	0.1
WR 140	WC7 + O4.5	–	1.67	2896.35	0.8964	1.0	4.1	1.0

Note. X-ray luminosity event signifiers: \Rightarrow at apastron; \uparrow at maximum; \downarrow at eclipse minimum. The orbital eccentricity is e .

fainter by an order of magnitude or more are the short-period WR 20a (O3If*/WN6+O3If*/WN6, $P = 3.686$ d) (Nazé, Rauw & Manfroid 2008), and the longer period WR 22 (WN7h+O9III-V, $P = 80.336$ d) (Gosset et al. 2009) although the phase coverage of these last two systems has been poor.

Even among colliding-wind binaries in general, Mk 34 is arguably the most luminous system yet identified. Also shown in Table 5 are comparisons with the brightest and best observed objects of this class, namely η Carinae (Hamaguchi et al. 2014; Corcoran et al. 2015, 2017), WR 140 (Pollock et al. 2005; Sugawara et al. 2015b) and WR 48a (Williams et al. 2012; Zhekov et al. 2014).

Despite much longer orbital periods of years and decades, all show X-ray cycles with many properties in common with Mk 34 with differences only of detail. In addition to a rich set of lines, spectra feature hard, bright X-ray continuum emission with equivalent temperatures of 4–5 keV. After minimum at apastron, luminosities rise gradually to maximum shortly before periastron before sudden, complex eclipses very close to periastron precede notably slow and asymmetric recoveries towards apastron and the beginnings of a new, usually repeatable cycle.

The only rival to Mk 34's status as the most X-ray luminous of the colliding-wind binaries is the LBV system η Carinae which displays several characteristics that are so far unique (Corcoran et al. 2015) including flares and eclipses of variable shape. It was during a flare in the approach to the most recent periastron passage in 2014 that η Carinae reached the exceptional maximum luminosity reported in Table 5 that was about 50 per cent higher than in previous cycles (Corcoran et al. 2017). For Mk 34, while the good agreement between the contrasts in count rate observed in comparison with *XMM-Newton* and *Swift* tends to suggest a reproducible maximum, data at maximum are sparse so that this should be subject to test with more *Chandra* data of high spatial resolution.

While Mk 34 is likely to be a system of two hydrogen-rich Wolf–Rayet stars, the high luminosity of η Carinae is supposed to be powered by interactions of a slow, dense LBV wind and the much faster wind of an unidentified companion. Nevertheless, given the obvious similarity of spectra and light curves, Mk 34 and η Carinae probably share many aspects of shock physics and geometry.

5 CONCLUSIONS

Mk 34 is one of the most prominent Wolf–Rayet stars in the LMC and the brightest stellar X-ray source. *Chandra* ACIS-I observations, made as part of the 2 Ms T-ReX campaign on the dense stellar cluster 30 Doradus, have revealed that it has a repeatable X-ray cycle of 155.1 d that is confirmed by archived *XMM-Newton* data and new ToO observations with *Swift*. It is the most X-ray luminous colliding-wind binary system yet identified, exceeding even η Carinae.

Though lacking coverage at some crucial phases, the form of the phased X-ray light curve of Mk 34 appears repeatable and very similar to the Galactic colliding-wind binary system WR 21a which is of shorter period and lower luminosity but whose more detailed light curve suggests that a combination of binary, geometrical and radiative mechanisms is responsible for the distinctive gradual rise to maximum before the sudden onset of a deep minimum and gradual recovery.

We are in the process of establishing the optical radial velocity orbit of Mk 34 in order to define how the geometrical disposition of the stars is related to its X-ray behaviour. Although located 50 kpc away in the LMC, Mk 34 is a brighter X-ray source most of the

time than many well-known Wolf–Rayet systems in the Galaxy. As a result, high-resolution observations with the *Chandra* HETG will also be feasible to confirm a variety of low metal abundances in the LMC and study the physics and dynamics of the shocks responsible for its X-rays. Detailed future X-ray photometry holds the promise of direct estimates of the radius of one or both of the stellar components of Mk 34, widely thought to be among the most massive of stars.

ACKNOWLEDGEMENTS

PSB, and LKT were supported by *Chandra X-ray Observatory* general observer (GO) grants GO5-6080X and GO4-15131X (PI: L. Townsley), and by the Penn State ACIS Instrument Team Contract SV4-74018, issued by the *Chandra* X-ray Center, which is operated by the Smithsonian Astrophysical Observatory for and on behalf of NASA under contract NAS8-03060. Partial financial support for AMTP and KT was provided by the United Kingdom STFC. We are very grateful to the *Swift* ToO program, its Project Scientist and Observatory Duty Scientists for awards of observing time, general support and extensive use of UKSSDC data analysis tools. This research has made use of SAOImage DS9, developed by Smithsonian Astrophysical Observatory.

REFERENCES

- Broos P. S., Townsley L. K., Feigelson E. D., Getman K. V., Bauer F. E., Garmire G. P., 2010, *ApJ*, 714, 1582
 Broos P. S. et al., 2011, *ApJS*, 194, 2
 Chené A.-N., Schnurr O., Crowther P. A., Fernández-Lajús E., Moffat A. F. J., 2011, in Neiner C., Wade G., Meynet G., Peters G., eds, *IAU Symp. Vol. 272, Active OB Stars: Structure, Evolution, Mass Loss, and Critical Limits*. Kluwer, Dordrecht, p. 497
 Corcoran M. F., 2005, *AJ*, 129, 2018
 Corcoran M. F. et al., 2015, preprint ([arXiv:1507.07961](https://arxiv.org/abs/1507.07961))
 Corcoran M. F. et al., 2017, *ApJ*, 838, 45
 Crowther P. A., Walborn N. R., 2011, *MNRAS*, 416, 1311
 Crowther P. A., Schnurr O., Hirschi R., Yusof N., Parker R. J., Goodwin S. P., Kassim H. A., 2010, *MNRAS*, 408, 731
 Crowther P. A. et al., 2016, *MNRAS*, 458, 624
 Doran E. I. et al., 2013, *A&A*, 558, A134
 Feldmeier A., Puls J., Pauldrach A. W. A., 1997, *A&A*, 322, 878
 Gosset E., Nazé Y., 2016, *A&A*, 590, A113
 Gosset E., Nazé Y., Sana H., Rauw G., Vreux J.-M., 2009, *A&A*, 508, 805
 Hainich R. et al., 2014, *A&A*, 565, A27
 Hamaguchi K. et al., 2014, *ApJ*, 784, 125
 Lomax J. R. et al., 2015, *A&A*, 573, A43
 Nazé Y., Rauw G., Manfroid J., 2008, *A&A*, 483, 171
 Nazé Y., Flores C. A., Rauw G., 2012, *A&A*, 538, A22
 Nazé Y., Oskinova L. M., Gosset E., 2013, *ApJ*, 763, 143
 Nichols J. et al., 2015, *ApJ*, 809, 133
 Niemela V. S., Gamen R. C., Barbá R. H., Fernández L. E., Benaglia P., Solivella G. R., Reig P., Coe M. J., 2008, *MNRAS*, 389, 1447
 Plavchan P., Jura M., Kirkpatrick J. D., Cutri R. M., Gallagher S. C., 2008, *ApJS*, 175, 191
 Pollock A. M. T., 2012, in Drissen L., Robert C., St-Louis N., Moffat A. F. J., eds, *ASP Conf. Ser. Vol. 465, Proceedings of a Scientific Meeting in Honor of Anthony F. J. Moffat*. Astron. Soc. Pac., San Francisco, p. 308
 Pollock A. M. T., Corcoran M. F., 2006, *A&A*, 445, 1093
 Pollock A. M. T., Corcoran M. F., Stevens I. R., Williams P. M., 2005, *ApJ*, 629, 482
 Portegies Z. S. F., Pooley D., Lewin W. H. G., 2002, *ApJ*, 574, 762
 Rauw G., Nazé Y., 2016, *Adv. Space Res.*, 58, 761
 Schnurr O., Casoli J., Chené A.-N., Moffat A. F. J., St-Louis N., 2008, *MNRAS*, 389, L38

- Skinner S. L., Zhekov S. A., Güdel M., Schmutz W., Sokal K. R., 2010, *AJ*, 139, 825
- Skinner S. L., Zhekov S. A., Güdel M., Schmutz W., Sokal K. R., 2012, *AJ*, 143, 116
- Stevens I. R., Blondin J. M., Pollock A. M. T., 1992, *ApJ*, 386, 265
- Sugawara Y., Tsuboi Y., Maeda Y., Pollock A. M. T., Williams P. M., 2015a, in Hamann W.-R., Sander A., Todt H., eds, *Proceedings of an International Workshop held in Potsdam, Germany, Wolf-Rayet Stars*. Universitätsverlag Potsdam, Potsdam, p. 366
- Sugawara Y. et al., 2015b, *PASJ*, 67, 121
- Townsley L. K., Broos P. S., Feigelson E. D., Garmire G. P., Getman K. V., 2006, *AJ*, 131, 2164
- Townsley L. K. et al., 2011, *ApJS*, 194, 1
- Townsley L. K., Broos P. S., Garmire G. P., Bouwman J., Povich M. S., Feigelson E. D., Getman K. V., Kuhn M. A., 2014, *ApJS*, 213, 1
- Tramper F., Sana H., Fitzsimons N. E., de Koter A., Kaper L., Mahy L., Moffat A., 2016, *MNRAS*, 455, 1275
- Williams P. M., van der Hucht K. A., van Wyk F., Marang F., Whitelock P. A., Bouchet P., Setia G. D. Y. A., 2012, *MNRAS*, 420, 2526
- Zhekov S. A., Tomov T., Gawronski M. P., Georgiev L. N., Borissova J., Kurtev R., Gagné M., Hajduk M., 2014, *MNRAS*, 445, 1663

This paper has been typeset from a $\text{\TeX}/\text{\LaTeX}$ file prepared by the author.